

Deep evolutionary origin of limb and fin regeneration

Sylvain Darnet^{a,1}, Aline C. Dragalzew^{a,1}, Danielson B. Amaral^{a,1}, Josane F. Sousa^a, Andrew W. Thompson^b, Amanda N. Cass^c, Jamily Lorena^{a,d}, Eder S. Pires^d, Carinne M. Costa^a, Marcos P. Sousa^e, Nadia B. Fröbisch^f, Guilherme Oliveira^d, Patricia N. Schneider^a, Marcus C. Davis^c, Ingo Braasch^b, and Igor Schneider^{a,2}

^aInstituto de Ciências Biológicas, Universidade Federal do Pará, 66075-900 Belém, Brazil; ^bDepartment of Integrative Biology, Program in Ecology, Evolutionary Biology, and Behavior, Michigan State University, East Lansing, MI 48824; ^cDepartment of Biology, James Madison University, Harrisonburg, VA 22807; ^dInstituto Tecnológico Vale, 66055-090 Belém, Brazil; ^eLaboratório de Biologia Molecular, Museu Paraense Emílio Goeldi, 66077-530 Belém, Pará, Brazil; and ^fMuseum für Naturkunde, Leibniz Institute for Evolution and Biodiversity Science, 10115 Berlin, Germany

Edited by Günter P. Wagner, Yale University, New Haven, CT, and approved June 11, 2019 (received for review January 10, 2019)

Salamanders and lungfishes are the only sarcopterygians (lobefinned vertebrates) capable of paired appendage regeneration, regardless of the amputation level. Among actinopterygians (rayfinned fishes), regeneration after amputation at the fin endoskeleton has only been demonstrated in polypterid fishes (Cladistia). Whether this ability evolved independently in sarcopterygians and actinopterygians or has a common origin remains unknown. Here we combine fin regeneration assays and comparative RNA-sequencing (RNA-seq) analysis of Polypterus and axolotl blastemas to provide support for a common origin of paired appendage regeneration in Osteichthyes (bony vertebrates). We show that, in addition to polypterids, regeneration after fin endoskeleton amputation occurs in extant representatives of 2 other nonteleost actinopterygians: the American paddlefish (Chondrostei) and the spotted gar (Holostei). Furthermore, we assessed regeneration in 4 teleost species and show that, with the exception of the blue gourami (Anabantidae), 3 species were capable of regenerating fins after endoskeleton amputation: the white convict and the oscar (Cichlidae), and the goldfish (Cyprinidae). Our comparative RNA-seq analysis of regenerating blastemas of axolotl and Polypterus reveals the activation of common genetic pathways and expression profiles, consistent with a shared genetic program of appendage regeneration. Comparison of RNA-seq data from early Polypterus blastema to single-cell RNAseq data from axolotl limb bud and limb regeneration stages shows that Polypterus and axolotl share a regeneration-specific genetic program. Collectively, our findings support a deep evolutionary origin of paired appendage regeneration in Osteichthyes and provide an evolutionary framework for studies on the genetic basis of appendage regeneration.

limb | fin | regeneration | tetrapod | evolution

A typical osteichthyan paired fin (i.e., pectoral and pelvic fin) is composed of an array of proximal fin radials (the endoskeleton), followed distally by the fin rays (the dermal skeleton). The tetrapod limb evolved from paired fins in Devonian sarcopterygians. During this transition, the fin ray dermal skeleton was lost and the elaborate limb endoskeleton emerged, consisting of a proximal segment, the stylopod (humerus and femur), an intermediate segment, the zeugopod (radius/ulna, tibia/fibula), and a distal segment, the autopod (manus and pes) (1). Therefore, whereas fin rays have no direct homologous counterpart in tetrapod limbs, the limb endoskeleton and the endoskeletal elements of fish paired fins share deep homology (2, 3) (Fig. 1.4).

Among sarcopterygians, the capacity to regenerate the limbs and fins after amputations severing the endoskeleton has been reported only in 3 groups: frogs (4), salamanders (5), and lungfishes (6). Although adult frogs cannot regenerate limbs, this capacity is exhibited by tadpoles before metamorphosis (7). Recent fossil evidence has shown that limb regeneration occurred in basal amphibians before the emergence of stem salamanders, caecilians, and frogs; hence, this capacity is likely an ancient, plesiomorphic feature of tetrapods (8, 9). Recently, transcriptome analysis revealed strong similarities between the transcriptional profiles deployed in lungfish fin and salamander limb blastemas (LBs) (6). Altogether, current

data support the hypothesis that tetrapods inherited a limb regeneration program from sarcopterygian fish ancestors (10).

Among actinopterygians, teleosts, such as zebrafish, have been broadly used for fin regeneration studies, yet their regenerative abilities are thought to be limited to the dermal fin ray skeleton (11, 12). However, evidence of tail regeneration after endoskeleton amputation has been shown in zebrafish (13). Thus far, only 2 actinopterygian species, both from the earliest branching ray-finned fishes, the Polypteridae, have been found to fully regenerate paired fins, including the endoskeleton: the Senegal bichir Polypterus senegalus (14, 15) and the ropefish Erpetoichthys calabaricus (15). Currently, our understanding of the evolution of appendage regeneration is hindered by limited knowledge of the regeneration capabilities across fish clades. To address this, we assessed fin regeneration capacity in key taxa representing all extant major actinopterygian clades and examined gene-expression profiles of limb and fin regenerating blastemas via RNA sequencing (RNA-seq) in Polypterus.

Here we provide evidence of regeneration after amputation at the fin endoskeleton in the American paddlefish (Chondrostei),

Significance

Salamanders and lungfishes are the only lobe-finned vertebrates where appendage regeneration after endoskeleton amputation has been demonstrated. Here we show that paired-fin regeneration after endoskeleton amputation occurs in living representatives of all major actinopterygian clades: the American paddlefish (Chondrostei), the spotted gar (Holostei), and in 2 cichlid and 1 cyprinid species (Teleostei). Through comparative transcriptome analysis of blastemas, we demonstrate that axolotl and *Polypterus* deploy a similar genetic program during regeneration. Furthermore, we show that early blastemas in both species activate a common regeneration-specific genetic program. Collectively, our findings support a deep evolutionary origin of limb and fin regeneration and highlight the strengths of a comparative approach to identify genetic signatures of vertebrate appendage regeneration.

Author contributions: S.D., A.C.D., D.B.A., J.F.S., A.W.T., A.N.C., N.B.F., M.C.D., I.B., and I.S. designed research; S.D., A.C.D., D.B.A., J.F.S., A.W.T., A.N.C., E.S.P., C.M.C., G.O., P.N.S., M.C.D., I.B., and I.S. performed research; S.D., J.L., E.S.P., C.M.C., M.P.S., G.O., P.N.S., M.C.D., and I.B. contributed new reagents/analytic tools; S.D., A.C.D., D.B.A., J.F.S., A.W.T., A.N.C., J.L., E.S.P., M.P.S., N.B.F., G.O., P.N.S., M.C.D., I.B., and I.S. analyzed data; and S.D., A.C.D., D.B.A., J.F.S., A.W.T., A.N.C., N.B.F., M.C.D., I.B., and I.S. wrote the paper.

The authors declare no conflict of interest

This article is a PNAS Direct Submission.

Published under the PNAS license.

Data deposition: The sequences reported in this paper have been deposited in the NCBI Sequence Read Archive (project nos. PRJNA480693 and PRJNA480698).

¹S.D., A.C.D., and D.B.A. contributed equally to this work.

²To whom correspondence may be addressed. Email: ischneider@ufpa.br.

This article contains supporting information online at www.pnas.org/lookup/suppl/doi:10.1073/pnas.1900475116/-/DCSupplemental.

Published online July 3, 2019.

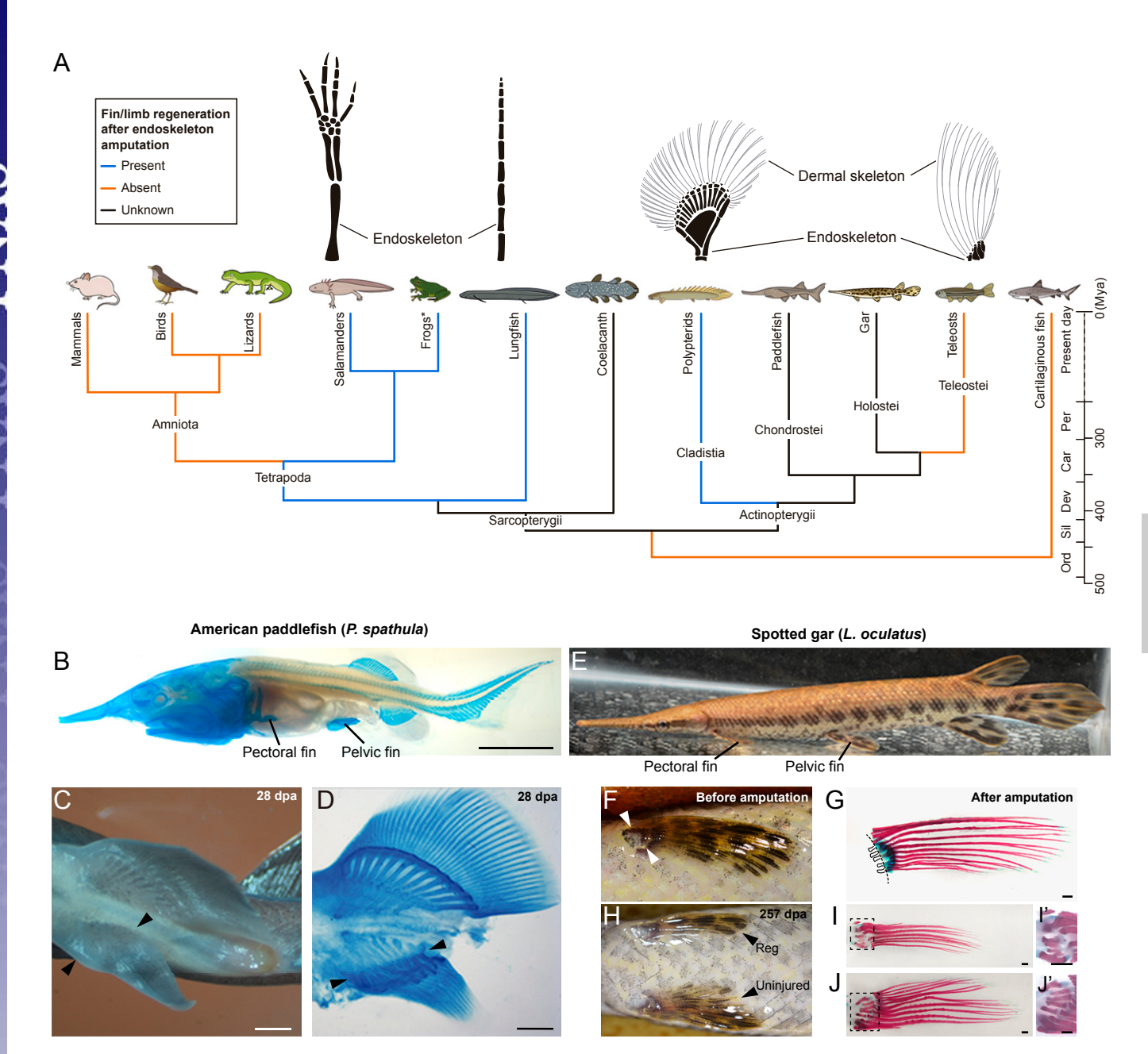


Fig. 1. Phylogenetic distribution of appendage regeneration after endoskeleton amputation among vertebrates and of fin regeneration in nonteleost actinopterygians. (A, Upper) Schematic representation of endoskeleton and dermal skeleton of vertebrate appendages. (A, Lower) A time-calibrated vertebrate phylogeny depicts the state of current knowledge at the time this study was undertaken. Lineages containing one or more species capable of fin or limb regeneration after endoskeleton amputation are denoted in blue, those incapable denoted in orange, and those where no information exists in black. (B) Cleared and stained juvenile paddlefish at 75 dpf; pectoral and pelvic fins denoted. (C) Ventral view of a specimen with regenerated right pelvic fin at 28 dpa; arrowheads denote amputation site. (D) Ventral view of the cleared and stained specimen shown in C, displaying endoskeletal regeneration distal to the amputation site. (E) Spotted gar with pectoral and pelvic fins denoted. (F) Left pelvic fin before amputation. (G) Skeletal staining of fin removed by amputation; dotted line shows amputation site across the endoskeleton. (H) Ventral view showing regenerated left fin at 257 dpa and uninjured right fin. (I') Skeletal staining of the regenerated fin. (I') Close-up view of uninjured right fin endoskeleton (Scale bars: 5 mm in B and 1 mm in C, D, G, I, I', J, and J'). Reg, regenerated. In panels B–J' anterior is to the left.

the spotted gar (Holostei), 2 cichlids, and 1 cyprinid (Teleostei), which together with polypterids (Cladistia), constitute living representatives of all major actinopterygian lineages. Furthermore, we show that regenerating blastemas of axolotl and *Polypterus* activate common genetic pathways and expression profiles. We also find that early blastema transcriptomes from *Polypterus* and axolotl deploy a shared regeneration-specific genetic program. Altogether, these findings suggest that regeneration of paired fins and limbs has a deep evolutionary origin.

Results

Fin Regeneration in Nonteleost Actinopterygians. The American paddlefish (*Polyodon spathula*) is a descendant of the early-diverging actinopterygian clade (Chondrostei, Acipenseriformes) (Fig. 1A). Paired fins of paddlefish are supported proximally by an elaborate endoskeleton. We chose to assess regeneration of pelvic fins, which have an endoskeleton compartment more readily accessible to amputations (Fig. 1B). We performed 8 pelvic fin amputations of juvenile fish and assessed regenerative growth 4 wk later (Fig.

1C). We found that at 28 d postamputation (dpa), 6 of 8 fish showed chondrogenic outgrowth and repatterning distal to the amputation plane (Fig. 1D). All specimens displayed heteromorphic regeneration, where the regenerated endoskeleton and dermal skeleton morphology differed from the original, with significant bifurcations of radials occurring at the amputation plane, as well as novel condensations and of cartilaginous bars (Fig. 1D and SI Appendix, Fig. S1 A-D). In 4 of 6 fish with regenerative outgrowths there was significant regrowth of the dermal fin-fold, including the formation of lepidotrichia. In sum, these results showed that juvenile paddlefish are capable of fin regeneration after amputation at the fin endoskeleton.

Gars (Lepisosteus oculatus) are members of the Lepisosteiformes (Holostei) and, together with polypterids and the chondrostean paddlefish, constitute living representatives of the 3 principal nonteleost clades of living actinopterygians (16) (Fig. 1A). We performed pectoral fin amputations across the endoskeleton (Fig. 1 E-G) on 15 individuals and followed regenerative outgrowth for ~8 mo. A total of 11 of 15 fish displayed various degrees of regeneration, from partial to near complete regrowth, and the regenerated fin radials and rays were often shorter and misshapen (Fig. 1 H–J' and SI Appendix, Fig. S1 E–H). Therefore, as seen in paddlefish, regeneration was mostly heteromorphic. Nevertheless, collectively, our results on gar and paddlefish, together with previous reports in polypterids, suggest that the capacity for regeneration after fin endoskeleton amputation is a common feature among living nonteleost actinopterygians.

Fin Regeneration After Endoskeleton Amputation in Teleosts. Given the observations above, the question of whether paired fin regeneration after endoskeleton amputation could extend to the teleost clade was reexamined. To this end, we selected 2 cichlid species, the white convict (Amatitlania nigrofasciata) and the oscar (Astronotus ocellatus), in which the pectoral fin endoskeleton compartment was sufficiently large and accessible for amputations (Fig. 2 A and E). As seen in gar, regeneration after amputation at the fin endoskeleton progressed slowly and was followed for several months. At 160 dpa, fin regeneration was observed in 6 of 8 white convicts (Fig. 2B and SI Appendix, Fig. S2 A and D). Similarly, 3 of 4 oscars showed fin regeneration at 90 dpa (Fig. 2F and SI Appendix, Fig. S2 G and J). In both species, the extent of regeneration varied, and regenerated fins differed from the original morphology. Skeletal staining of the amputated fins confirmed that amputation planes crossed the fin endoskeletons, removing the distal ends of the radials (Fig. 2 C and G and SI Appendix, Fig. S2 H and K). In white convicts, regenerated fin radials displayed discrete distal outgrowth and some radials partially recovered the original morphology (Fig. 2 D and D' and SI Appendix, Fig. S2 C, C', F, and F'). Fin radial distal outgrowth was occasionally associated with hypertrophy and the regenerated dermal skeleton was characterized by fin rays that were shorter and reduced in number (Fig. 2D' and SI Appendix, Fig. S2 C' and F'). In oscars, regenerated fin radials also showed distal outgrowth and hypertrophy and fin rays were shorter and reduced in number (Fig. 2 H and H' and SI Appendix,

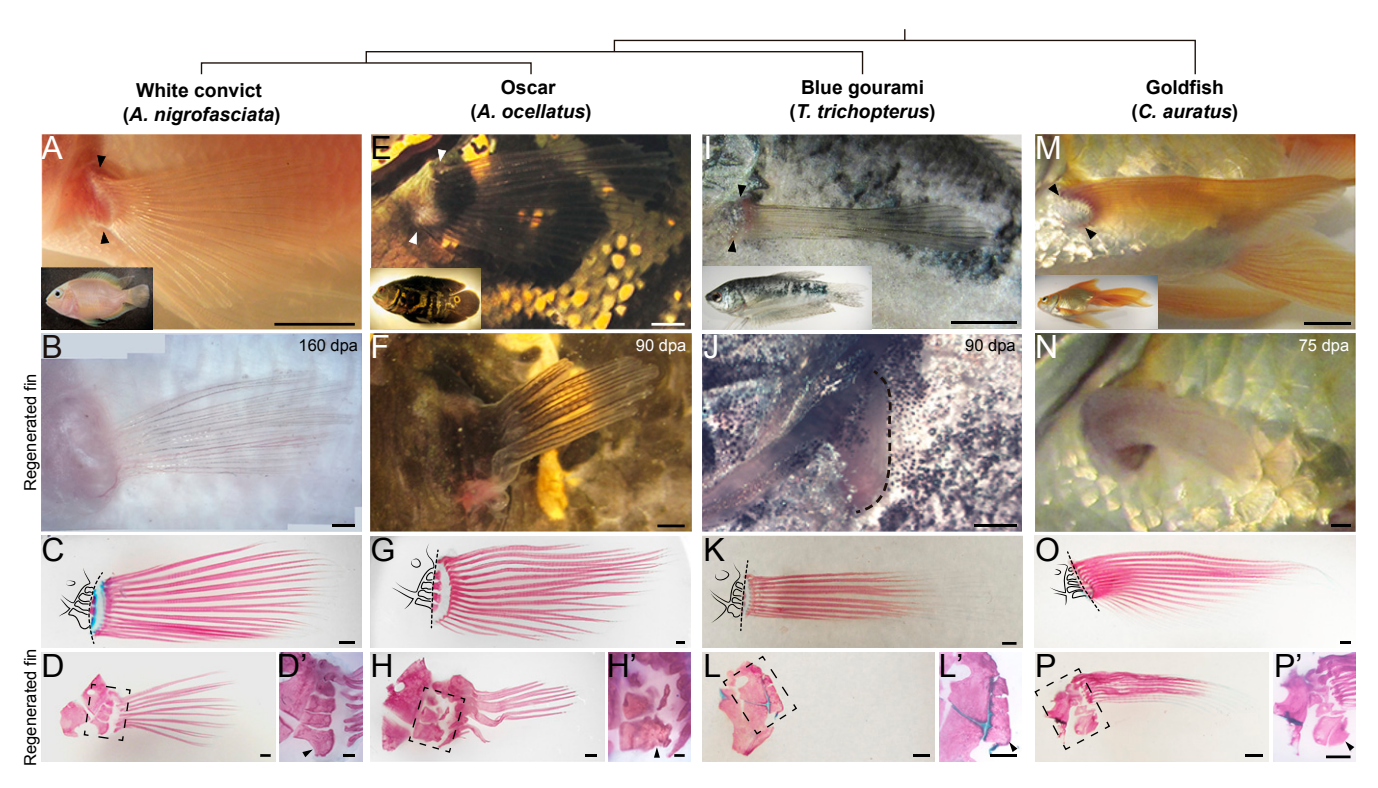


Fig. 2. Evidence of regeneration after endoskeletal fin amputation in teleosts. (A) Side view, white convict specimen (Inset) and its left pectoral fin; arrowheads denote amputation site. (B) Regenerated fin at 160 dpa. (C) Skeletal staining of fin removed by amputation; dotted line denotes amputation site across the endoskeleton. (D) Skeletal staining of the regenerated fin at 160 dpa. (D') Close-up view of the regenerated endoskeleton. (E) Side view, oscar specimen (Inset) and its left pectoral fin; arrowheads denote amputation site. (F) Regenerated fin at 90 dpa. (G) Skeletal staining of fin removed by amputation; dotted line shows amputation site across the endoskeleton. (H) Skeletal staining of the regenerated fin at 90 dpa. (H') Close-up view of the regenerated endoskeleton. (I) Side view, blue gourami specimen (Inset) and its left pectoral fin; arrowheads denote amputation site. (I) Fin at 90 dpa, black dashed line denotes edge of fin stump. (K) Skeletal staining of fin removed by amputation; dotted line shows amputation site across the endoskeleton. (L) Skeletal staining of the fin at 90 dpa. (L') Close-up view of the endoskeleton. (M) Side view, goldfish specimen (Inset) and its left pectoral fin; arrowheads denote amputation site. (N) Regenerated fin at 75 dpa. (O) Skeletal staining of fin removed by amputation; dotted line shows amputation site across the endoskeleton. (P) Skeletal staining of the regenerated fin at 75 dpa. (P') Close-up view of the regenerated endoskeleton (Scale bars: 5 mm in A, E, I, and M; 1 mm in B-D', F-H', J-L', and N-P'). Arrowheads indicate endoskeleton (D', H', L', and P').

Fig. S2 I, I', L, and L'). Altogether, these results demonstrate that despite being predominantly heteromorphic, regeneration of paired fins following amputation through the endoskeleton is observed in these cichlids.

To further expand our sampling across teleosts, we selected 2 additional species for regeneration assays: the blue gourami Trichogaster trichopterus (Anabantiformes) and the goldfish Carassius auratus (Cypriniformes), whose lineages are estimated to have diverged from the Cichliformes 117 and 230 Mya, respectively (17). We assayed 7 blue gouramis for the ability to regenerate after amputation at the endoskeleton level (Fig. 2 I-K and SI Appendix, Fig. S2 M-O'). However, fin outgrowth was not observed in amputated fins at 90 dpa (Fig. 2 L and L'). Goldfish, however, were capable of fin regeneration after endoskeletonlevel amputations (n = 9) (Fig. 2 M–O and SI Appendix, Fig. S2 S-X'). At 75 dpa, regenerated goldfish fins had new endoskeletal elements and fin rays, although the endoskeletal elements were shorter and hypertrophied and the fin rays were reduced in number and length (Fig. 2 P and P'). Importantly, evidence of regenerative fin outgrowth was observed in regenerationcompetent teleosts (white convict, oscar, and goldfish) as early as 30 dpa (SI Appendix, Fig. S2Y).

Overall, our findings showed that fin regeneration after amputation at the endoskeleton is found in representatives of all major living actinopterygian clades. We interpret these findings as best fitting a scenario where fin regeneration after endoskeleton amputation is a complex ancestral trait that has been subsequently retained in some species, such as those shown to be regeneration-competent in our assays. In this scenario, blue gouramis and other regeneration-incompetent species represent loss of regeneration capacity. Together with previous reports in salamanders and lungfish, our findings are consistent with the hypothesis that the ability to regenerate appendages after endoskeleton amputation was likely already present in Osteichthyes before the divergence of the actinopterygian and sarcopterygian lineages.

Axolotl and Polypterus Deploy Common Genetic Pathways during Appendage Regeneration. Given our findings, we hypothesized that actinopterygian fins and salamander limbs may share a common, ancient genetic program for appendage regeneration. To examine this, we generated RNA-seq data from *Polypterus* fin blastema (FB) and uninjured fin (UF), and axolotl LB and uninjured limb (UL) (SI Appendix, Fig. S3 A-D). We produced 3 independent RNA-seq libraries from pools of Polypterus UF and FB at 9 dpa (18), a stage where new cartilage condensation is starting to form (14) (see, for example, Fig. 5B). We also generated 3 independent RNA-seq libraries from pools of axolotl UL and LB at 14 dpa (19), equivalent to a medium-late bud stage (20). Spearman correlation coefficients among biological replicas were greater than 0.71, corroborating the reproducibility of RNA-seq runs (SI Appendix, Fig. S3E). Reads from all runs were used to produce de novo assemblies of reference transcriptomes for both *Polypterus* and axolotl (SI Appendix, Fig. S3F). Differential gene expression (DGE) analysis of the axolotl LB vs. UL revealed 562 down-regulated and 1,443 up-regulated genes. Our axolotl DGE data correlate well to publicly available axolotl limb regeneration RNA-seq profiles, with up- and downregulated genes showing equivalent transcripts per million (TPM) values in all RNA-seq replicas (21) (SI Appendix, Fig. S4) A and B and Datasets S1 and S2). Next, we performed DGE analysis of the Polypterus FB vs. UF and found 379 downregulated and 957 up-regulated genes, including genes typically down-regulated (Mybpc2, Casq1, Myoz1, Smpx, Tnnt3) or upregulated (Mmp11, Sall4, Msx2, Sp9, Wnt5a, Fgf8, and Fgf10) in axolotl blastemas (22–26) (Fig. 3A and Dataset S2). qPCR profiles of 12 differentially expressed targets were largely consistent with the Polypterus RNA-seq data (SI Appendix, Fig. S4C). Our comparison of axolotl and Polypterus blastema DGE datasets revealed that

35.31% of the genes up-regulated in the *Polypterus* FB possess homologs up-regulated in the axolotl LB as well (Fig. 3B). To determine the expected overlap between the 2 DGE datasets by chance, we produced 1,000 lists containing 957 Polypterus genes randomly sampled from the 14,274 genes annotated in our Polypterus reference transcriptome. We found that the mean percent overlap expected by chance is 9.36%. When we computed the percent overlap into a z-score, which measures how many SDs the percent overlap between our Polypterus FB and axolotl LB is above the random expected mean, we found that the 35.31% overlap corresponds to a z-score of 21.38, and is significantly different from the expected overlap by chance (Fig. 3C). Next, we performed a gene set enrichment analysis (GSEA) to compare appendage regeneration signatures of axolotl LB to our Polypterus DGE dataset. Our analysis revealed that genes overexpressed in our axolotl LB dataset were significantly enriched among genes up-regulated in the *Polypterus* FB (Fig. 3D). Analysis of enriched gene ontology (GO) categories showed that Polypterus blastema is enriched for several GO terms also associated with axolotl LB, including appendage morphogenesis, extracellular matrix organization, and chromatin remodeling (Dataset S3). Furthermore, we found that 179 of 265 (67.54%) of the enriched GO categories in the Polypterus blastema were also enriched in the axolotl blastema transcriptome (Fig. 3B).

Next, we performed a pathway overrepresentation analysis on the blastema up-regulated genes in Polypterus and axolotl. A graphical representation of this data shows each top-level pathway as a central circle, connected to other circles representing the next level lower in the pathway hierarchy (Fig. 3E; see zoomin on a section of the cell cycle pathway). Our analysis revealed that 88.1% (155 of 176) and 88.7% (118 of 133) of enriched pathways in Polypterus and axolotl, respectively, fall into 7 of 26 broader categories, namely extracellular matrix organization, cell cycle, DNA replication, DNA repair, metabolism of proteins, metabolism of RNA, and gene expression (transcription). We found that 90 of 133 (67.7%) overrepresented pathways in axolotl LB were shared with the Polypterus FB dataset, including pathways involved in collagen formation, extracellular matrix organization, regulation of TP53 activity, and cell cycle. Conversely, among down-regulated genes, we found that 14 of 28 (50.0%) shared overrepresented pathways between Polypterus and axolotl, including pathways involved in muscle contraction and metabolism (SI Appendix, Fig. S5 and Dataset S4). Collectively, our findings revealed substantial similarities of gene expression, GO enrichment, and pathway overrepresentation profiles between *Polypterus* and axolotl blastemas.

Axolotl and Polypterus Early Blastemas Share a Genetic Appendage Regeneration Program. Various signaling pathways deployed during axolotl limb regeneration are also activated during limb development, suggesting that regeneration largely recapitulates development (27). A recent single-cell RNA-seq (scRNA-seq) analysis comparing axolotl LBs to developing limb buds found a high correlation between gene-expression profiles of late-stage LBs and developing limb buds. On the other hand, early-stage 3-dpa and 5-dpa axolotl blastemas showed a more unique, regeneration-specific gene-expression profile (28). To determine whether *Polypterus* and axolotls deploy a common regenerationspecific genetic program during early stages of regeneration, we generated transcriptome data for Polypterus early fin blastema (EFB) at 3 dpa (18), when the regenerated tissue lacks any noticeable cartilage condensation (see, for example, Fig. 5A). Pools of 3-dpa blastemas were used to generate 3 RNA-seq libraries, and reads were subsequently mapped to our Polypterus reference transcriptome (SI Appendix, Fig. S3 A-D). Spearman correlation coefficients among replicas were greater than 0.84, attesting to the reproducibility of RNA-seq runs (SI Appendix, Fig. S3E). DGE analysis of the Polypterus 3 dpa vs. Polypterus UF showed

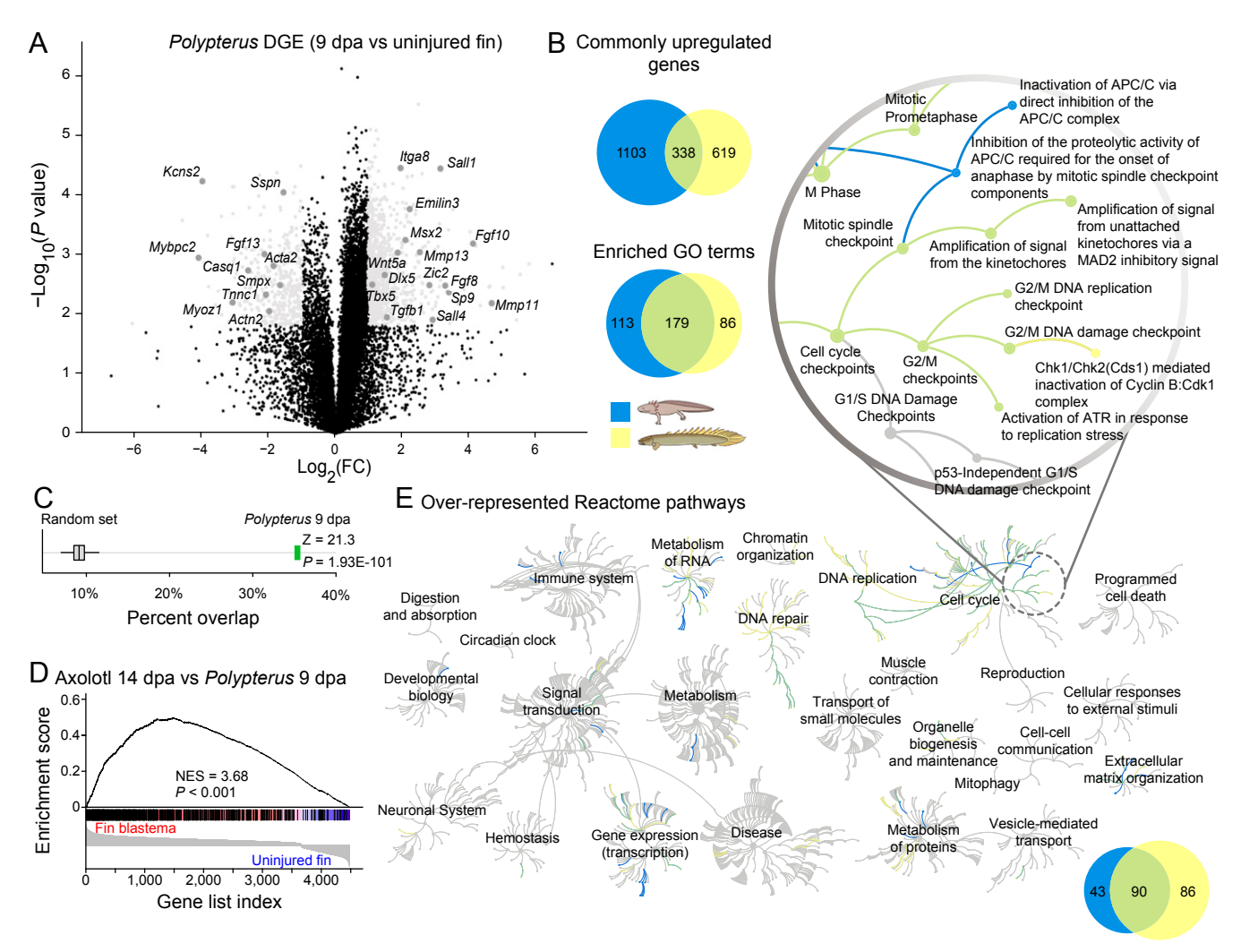


Fig. 3. Comparative transcriptome analysis of *Polypterus* fin and axolotl LB. (A) Volcano plot showing DEGs in *Polypterus* between UF tissue and 9-dpa FB (P < 0.05, FC > |2|), *Polypterus* orthologs commonly up or down-regulated in axolotl blastema are noted. (B) Area-proportional Venn diagrams showing upregulated genes (P < 0.05, FC > 2) and enriched GO categories (P < 0.05) in axolotl and *Polypterus* DGE datasets. (C) Observed percent overlap between the DGE datasets relative to the expected mean overlap by chance. (D) GSEA comparison of appendage regeneration signatures of axolotl LB relative to the *Polypterus* 9-dpa DGE dataset. (E) A graphical overview of Reactome pathway analysis for axolotl and *Polypterus*; each of the central circles is a top-level pathway and each step away from the center represents a lower level in the pathway hierarchy (see *Upper Right* for a zoom of a section of the top-level pathway cell cycle). Overrepresented pathways (P < 0.05) are colored in yellow (*Polypterus*), blue (axolotl), or green (overlayed pathways from both species); light gray represents pathways not significantly overrepresented. *Inset* (*Lower Right*) shows the area-proportional Venn diagram of the enriched pathways in both species.

3,554 genes up-regulated and 705 genes down-regulated (Fig. 4A and Dataset S2). Among the up-regulated DGE dataset, we detected many genes previously found up-regulated during early regeneration, such as *Hmox1*, *Steap1*, *Fgf10*, *Tgfb1*, *Msx2*, *Mmp8*, and *Il11* (Fig. 4A). Other genes previously implicated in axolotl limb regeneration in candidate gene studies, in high-throughput assays, as well as genes involved in both development and regeneration were also up-regulated in the *Polypterus* 3-dpa DGE dataset, such as *Fen1*, *Nrg1*, *Tp53*, *Cirbp*, *Hoxa9*, *Tgfa*, *Mmp11*, and *Cxcl8* (*Il8*) (26, 28, 29).

Early stages of salamander limb regeneration are characterized by an inflammatory response associated with macrophage recruitment and up-regulation of cytokines, such as II-1 (30). Recently, II-8 was found to be required for axolotl limb regeneration (29). Signaling via reactive oxygen species (ROS) has also been identified to be among the earliest cues involved in the initiation of limb and tail regeneration in salamanders and *Xenopus* (31–33). To determine which pathways were enriched in

Polypterus EFB vs. FB, we compared overrepresented pathways in 3-dpa and 9-dpa Polypterus DGE datasets (Dataset S4). A graphical representation of these data revealed the most distinctive top-level pathway categories among each dataset (Fig. 4B and SI Appendix, Fig. S5). Polypterus 9-dpa blastema showed strong overrepresentation of pathways in DNA repair (such as mismatch repair and processing of DNA double-stranded break ends), which was not observed in 3-dpa blastema (Fig. 4B). Conversely, overrepresented pathways in the *Polypterus* 3-dpa blastema were found in the broader categories of the immune system (such as IL-1 signaling), signal transduction (such as degradation of Axin and degradation of Gli1 by the proteasome), and cellular responses to external stimuli (such as cellular response to stress, which includes components of ROS signaling) (Fig. 4B). Overall, the DGE and overrepresented pathway profiles of Polypterus 3-dpa blastema show activation of signaling programs previously implicated in limb regeneration initiation in axolotl.

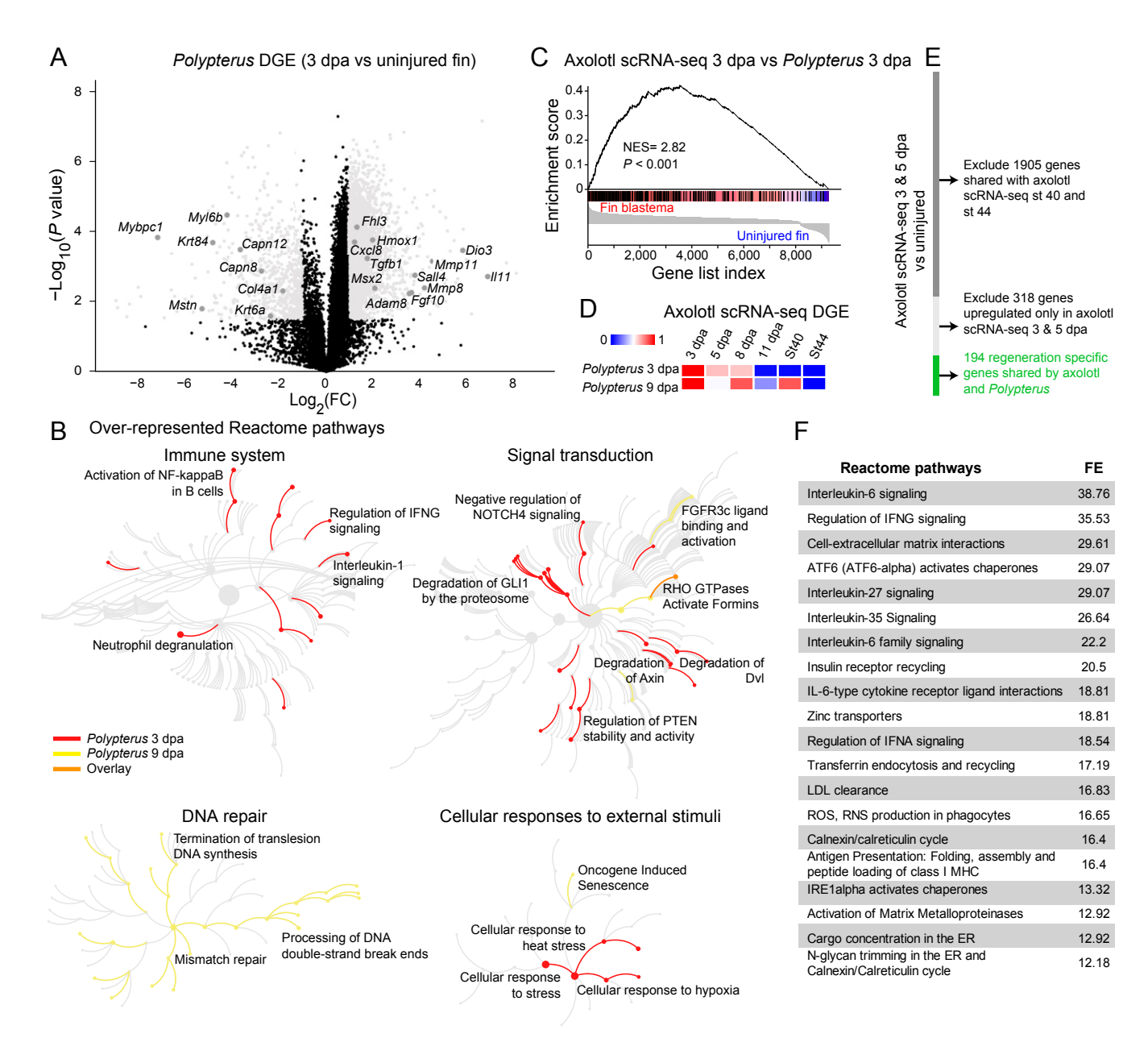


Fig. 4. Identification of a shared appendage regeneration genetic program in axolotl and *Polypterus* early blastemas. (A) Volcano plot showing DEGs in *Polypterus*, between UF tissue and 3-dpa EFB (P < 0.05, FC > |2|), *Polypterus* orthologs up- or down-regulated in early blastema are noted. (B) Graphical overview of Reactome pathways overrepresented (P < 0.05) in *Polypterus* 3 dpa (red) and 9 dpa (yellow) or on both stages (overlay: orange); light gray represents pathways not significantly overrepresented. (C) GSEA comparison of appendage regeneration signatures of the axolotl 3-dpa scRNA-seq DGE dataset relative to the *Polypterus* 3-dpa DGE dataset. (D) Heatmap of similarity between GSEA enrichment scores from comparisons of axolotl scRNA-seq datasets from Gerber et al. (28) to the *Polypterus* 3- and 9-dpa DGE dataset. (E) Schematic representation of filtering steps leading to a gene list shared by axolotl 3- and 5-dpa scRNA-seq DGE and *Polypterus* 3-dpa DGE datasets. (F) Top 20 overrepresented Reactome pathways and respective fold-enrichment (FE) values from the 194 regeneration-specific genes found in E.

Next, we sought to determine which axolotl blastema or developmental stage best correlates with our 3-dpa *Polypterus* DGE dataset. To achieve this, we used publicly available axolotl scRNA-seq data to generate mock transcriptomes in which a gene's TPM value corresponds to the mean TPM value obtained from all sequenced cells in each condition. Mock transcriptomes were made for scRNA-seq data from LB stages (3, 5, 8, and 11 dpa) and limb bud developmental stages (St40 and St44) (28). Then, we created DGE datasets of genes up-regulated in each of the above-mentioned regeneration and developmental stages relative to the scRNA-seq mock transcriptome corresponding to the uninjured 0-dpa limb (Dataset S5). Next, we used GSEA to find

which axolotl DGE dataset best correlates to our *Polypterus* 3- and 9-dpa DGE datasets. Our analysis showed that the highest enrichment score is obtained when comparing our *Polypterus* 3-dpa DGE to the axolotl scRNA-seq 3-dpa DGE dataset (Fig. 4 *C* and *D*), with decreasing enrichment scores for later axolotl regeneration stages (5, 8, and 11 dpa) and for limb bud stages (St40 and St44) (*SI Appendix*, Fig. S6). Whereas our *Polypterus* 9-dpa DGE dataset also showed high enrichment score compared with 3- and 8-dpa axolotl scRNA-seq DGE, a comparably high score was also seen for the comparison with limb bud St40 scRNA-seq DGE (Fig. 4*D*). We concluded that in contrast to the 9-dpa blastema, the *Polypterus* 3-dpa blastema correlates

better with early axolotl blastemas than with developing axolotl limb bud DGE datasets.

To identify a putative regeneration-specific genetic program shared by Polypterus and axolotl, we first sought to subtract from the axolotl blastema DGE datasets those genes up-regulated in limb bud DGE datasets. To this end, we combined the upregulated gene list of axolotl scRNA-seq 3- and 5-dpa DGE dataset, which added up to 2,417 genes. From this list we removed 1,905 genes corresponding to genes also found up-regulated in limb bud St40 and St44 DGE datasets. In the remaining 512 genes, which correspond to the axolotl regeneration-specific gene list, we found that 194 genes were shared with the Polypterus 3-dpa DGE dataset (Fig. 4E and Dataset S5). Pathway overrepresentation analysis showed that this shared set of regeneration-specific genes between *Polypterus* and axolotl is enriched for pathways, such as IL-6 signaling, cell-extracellular matrix interactions, ROS signaling, and activation of matrix metalloproteinases (Fig. 4F and Dataset S6). These results show that *Polypterus* and axolotl deploy a common, regeneration-specific genetic program in early-stage blastemas.

Regeneration-Specific Expression Pattern of Select Genes in Polypterus Early and Late Blastemas. Finally, we sought to assess the spatial patterns of expression of genes found in our Polypterus DGE datasets by in situ hybridization in histological sections of blastemas at 3 and 9 dpa (Fig. 5 A and B). Msx1 encodes a homeobox transcription factor capable of inducing dedifferentiation of myotubes (34), is up-regulated during limb regeneration in salamanders (24, 26, 35), and is expressed in blastema mesenchymal cells of *Xenopus* froglets (36). Similarly, we detected Msx1 expression in the Polypterus blastema mesenchyme at 3 dpa, and also in mesenchymal cells near the amputation site at 9 dpa (Fig. 5 C and D). Fgf10 expression has been detected in regenerating blastema mesenchyme of Xenopus froglets and axolotl (36, 37). As seen in amphibian blastemas, Fgf10 was expressed in mesenchymal cells in the 3-dpa blastema (Fig. 5E). At 9 dpa, signal was seen in mesenchymal cells near the amputation site and did not extend to the regenerating fin fold (Fig. 5F). Adam8 encodes a metalloprotease associated with skeletal muscle regeneration (38). Adam8 has not been previously linked to limb regeneration. However, it was found upregulated in our *Polypterus* 3 dpa and axolotl scRNA-seq 3- and 5-dpa DGE datasets. Our results show Adam8 highly and broadly expressed in blastema cells and cells proximal to the amputation site at 3 dpa (Fig. 5G). At 9 dpa, expression is restricted to a few mesenchymal cells along the regenerating blastema (Fig. 5H). Dio3 encodes a deiodinase that catalyzes the inactivation of the thyroid hormone and is up-regulated in *Polypterus* 3 dpa and axolotl scRNA-seq 3- and 5-dpa DGE datasets. In mice, satellite cell-specific genetic ablation of Dio3 impairs skeletal muscle regeneration (39). We detected scattered Dio3 expression in mesenchymal cells proximal and distal to the amputation site at 3 dpa (Fig. 51). At 9 dpa, Dio3 expression is mostly distal to the amputation site and discretely detected in mesenchymal and epithelial cells along the regenerating fin fold (Fig. 5J). Finally, Runx1 encodes a runt-related transcription factor required for myoblast proliferation during muscle regeneration in mice (40) and up-regulated during limb regeneration in salamanders (41). At 3 dpa, we detect Runx1 expression in the blastema and in cells proximal to the amputation site (Fig. 5K). At 9 dpa, Runx1 signal is detected in mesenchymal cells near the amputation site, at the base of the regenerating fin fold, and does not extend distally (Fig. 5L). In situ hybridization with control sense probes did not yield signal (SI Appendix, Fig. S7). In sum, our results revealed the expression patterns of genes implicated in both *Polypterus* and axolotl appendage regeneration and showed that Msx1 and Fgf10 expression in Polypterus blastema resembles the expression patterns described in axolotl and Xenopus froglets.

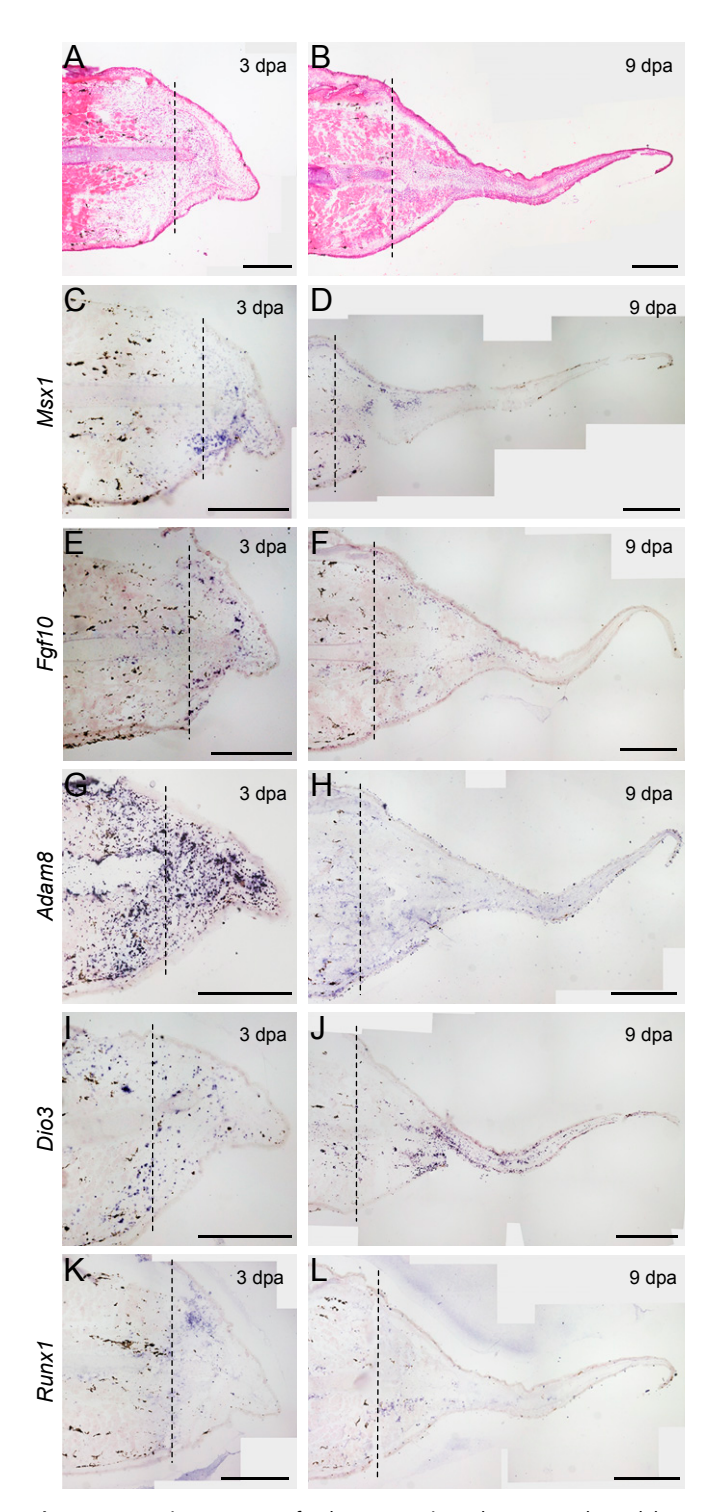


Fig. 5. Expression pattern of select genes in Polypterus early and late blastemas. Longitudinal histological sections of Polypterus blastemas at 3 dpa (A, C, E, G, I, and K) and 9 dpa (B, D, F, H, J, and L); all panels show posterior view, dorsal to the top. (A and B) H&E staining. (C-L) In situ hybridizations show expression patterns of Msx1, Fgf10, Adam8, Dio3, and Runx1. Dotted lines indicate amputation site (Scale bars, 1 mm in all panels).

Discussion

Here we provide evidence of a wide phylogenetic distribution of appendage regeneration after endoskeleton amputation across diverse fish lineages (Fig. 6). In all species examined, the morphology of regenerated fins differed substantially from uninjured

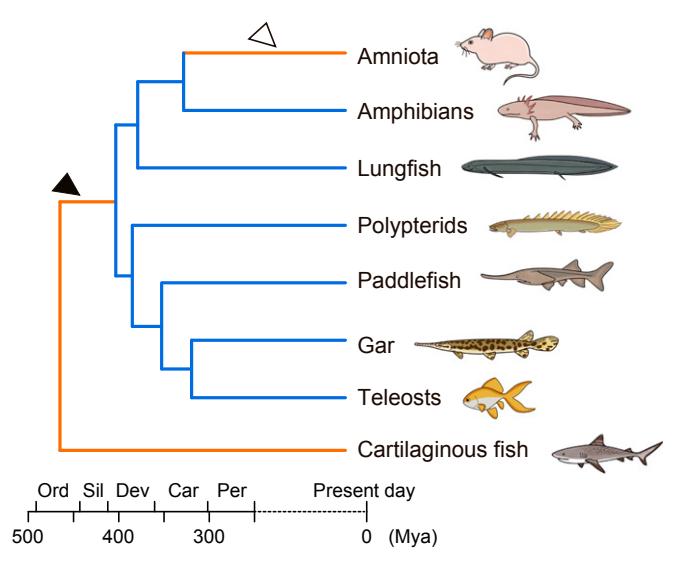


Fig. 6. Hypothesis for the evolution of limb and fin regeneration after endoskeleton amputation in vertebrates. Regeneration-incompetent lineages are shown in orange, lineages with one or more regeneration-competent species are shown in blue; black arrowhead indicates the origin of paired fin regeneration and white arrowhead loss of limb regeneration.

fins. Heteromorphic regeneration has been previously reported for salamanders (42), lungfish (6), and dermal fin ray regeneration in teleosts (43). Repeated fin amputations also result in abnormal endoskeleton morphologies in *Polypterus* (15). In our study, all 5 regeneration-competent species examined showed varying degrees of heteromorphic regeneration. These findings suggest that a great variability of fin regenerating capacity may exist among actinopterygians. Nevertheless, in the species examined, regenerative outgrowth was the most common outcome of fin amputation at the endoskeleton level.

Extensive taxonomic sampling is essential to establish the direction of evolutionary change. In addition to our data in nonteleosts, we present data from 3 teleost species (2 cichlids and goldfish) representing lineages that split over 230 Mya (17), in which amputation at the pectoral fin endoskeleton resulted in heteromorphic fin regeneration. It is important to note that, as we observed in blue gouramis, lack of regenerative capacity may be widespread in teleosts. However, because Anabantiformes (and teleosts in general) are nested within regeneration-competent clades, we argue that secondary loss of regenerative capacity is the most likely scenario in blue gouramis or other potential teleost species lacking fin regenerative capacity. Presence of regeneration in a species may also result from reacquisition of regenerative capacity. In the end, additional taxonomical sampling and regeneration assays will aid in establishing the polarity of evolutionary change within fish lineages and possibly provide a valuable source of new research organisms for comparative studies of appendage regeneration.

Our transcriptome comparisons showed significant similarities in gene-expression profiles between *Polypterus* and axolotl blastemas. In agreement with our findings, a recent transcriptome study showed that the *Polypterus* 4-dpa blastema triggers a similar genetic program to that described in axolotl and lungfish appendage regeneration (44). Here we show that many genes and pathway-detected *Polypterus* 9-dpa blastema are also observed during axolotl regeneration. However, as shown in a recent study (28), late blastemas also display significant similarity to the genetic program of limb buds. Conversely, we also show that the genetic program deployed in the *Polypterus* 3-dpa blastema compares best to 3-dpa axolotl blastema, and pathways traditionally associated

with initiation of limb regeneration, such as expression of cytokines and ROS signaling, were also detected in the *Polypterus* early blastema. Our in situ hybridizations in *Polypterus* blastemas show mesenchymal expression of *Msx1* and *Fgf10*, as seen in blastemas of axolotls and *Xenopus* froglets. Furthermore, we also provide expression patterns in *Polypterus* blastemas for genes previously implicated in axolotl limb regeneration.

In our compiled list of 194 regeneration-specific genes commonly deployed by Polypterus and axolotl, we have excluded genes up-regulated during axolotl limb bud stages. However, it is important to note that developmental genes may have regeneration-specific roles in addition to those identified in the context of development. In mice where Shh has been genetically inactivated (45) or in developing salamanders treated with the Shh inhibitor cyclopamine (46), the stylopod and zeugopod form, and only the digits are affected. During axolotl limb regeneration, however, continuous Shh inhibition blocks regeneration entirely, and a limb does not form (47, 48), suggesting that Shh plays a role in the initiation of limb regeneration distinct from its role during autopod development. Fgf10, expressed in the apical ectodermal ridge during development, is expressed in mesenchymal cells during limb regeneration in axolotl, and in Xenopus froglets expression is dependent on nerve supply (36).

In conclusion, the search for genes linked to fin and limb regeneration has been mostly pursued without a well-founded evolutionary context. If fin and limb regeneration have a common evolutionary origin, then genes facilitating regeneration in extant species are likely part of an ancient genetic program, whereas species without the capacity likely lost this ability over evolutionary time. Furthermore, gain or loss of *cis*-regulatory elements controlling a regeneration-specific gene-expression profile may explain the broad yet uneven distribution of appendage regeneration in animals. Therefore, an evolutionarily informed approach based on the comparative analysis of regenerating limbs and fins will offer a more powerful method to identify a shared genetic program underlying vertebrate appendage regeneration, providing a prime target for future biomedical intervention.

Methods

Animal Work. Polypterus (P. senegalus), oscar (A. ocellatus), white convict (A. nigrofasciata), goldfish (C. auratus), and blue gourami (T. trichopterus) were maintained in individual tanks in a recirculating freshwater system at 24 to 28 °C with aeration. All animals used were anesthetized in 0.1% MS-222 (Sigma) before amputations. Experiments and animal care were performed following animal care guidelines approved by the Animal Care Committee at the Universidade Federal do Para (protocol no. 037-2015). Axolotls (Ambystoma mexicanum) were obtained from the Center for Regenerative Therapies (Dresden, Germany) and maintained in accordance with the animal care guidelines at the Museum für Naturkunde Berlin (Germany). Paddlefish (P. spathula) embryos were obtained from Osage Catfisheries (Osage Beach, MO), and were raised at 18 °C in recirculating large-volume freshwater tanks, in accordance with approved Institutional Animal Care and Use Committee (IACUC) protocols at Kennesaw State University (protocol no. 16-001; former institution of M.C.D.), and James Madison University (protocol no. A19-02). Spotted gar (L. oculatus) were obtained as embryos from hormone-induced spawns of wild-caught broodstock from bayous near Thibodaux, Louisiana, raised in 150- to 300-gallon tanks, in accordance with approved Institutional IACUC protocols at Michigan State University (protocol no. AUF 10/16-179-00).

Pectoral fins of *Polypterus* fish ranging from 5 to 8 cm (n=30) were bilaterally amputated across the endoskeleton. A portion of the amputated fins, encompassing the endoskeleton elements, was sampled and labeled as UF tissue (n=6), and FB tissue was sampled from the left and right fins at 3 dpa (n=14) and 9 dpa (n=10). Fish were killed in 300 mg/L of MS-222 (Sigma). Samples were used for histology or stored in RNAlater (Sigma) for RNA extraction and subsequent qPCR or RNA-seq experiments. Axolotts ranging from 8 to 12 cm (n=6) were anesthetized in 0.1% MS-222 (Sigma) and forelimbs were bilaterally amputated at the level of the upper arm. A portion of the upper arm tissue was sampled and labeled as UL, and LB tissue was sampled at 14 dpa (n=6: 3 pools of 2 individuals each). All tissues collected were stored in RNAlater (Sigma) for RNA extraction and

subsequent RNA-seq experiments. Juvenile paddlefish (n = 8) were anesthetized in 0.1% MS-222 (Sigma) at 48 d postfertilization (dpf) and pelvic fin amputations were performed (49). Fish were raised for 28 dpa, to a total length of 8 to 13 cm, then killed with a lethal dose of MS-222 (Sigma), fixed in 4% paraformaldehyde (PFA) in PBS, and stored in methanol at $-20~^{\circ}\text{C}$ until analysis. Specimens were cleared and stained as previously described (49) and photographed with a Zeiss SteREO Discovery.V12 microscope with MRc5 camera. Gar ranging from 20 to 27 cm in total length and between 263 and 298 dpf were anesthetized with 160 mg/L MS-222 (Sigma), tagged with uniquely numbered Floy tags, and the left pectoral fin was amputated at the endoskeleton level. Fins were fixed in 2% PFA in PBS and stored in 80% ethanol. Pectoral fin regeneration (n = 15) was documented with a Nikon D7100 DSLR camera and a 40-mm macro lens. Fish were sampled at various stages of regrowth following killing in 300 mg/L MS-222 (Sigma). Four oscars (10 to 15 cm), 8 white convicts (6 to 8 cm), 9 goldfish (9 to 10 cm), and 7 blue gouramis (8 to 10 cm) were used in this study. Pectoral fins were amputated at the endoskeleton level. Sampled fins were fixed 4% PFA in PBS for subsequent skeletal preparation. Regeneration was assessed at 75 dpa in goldfish, at 90 dpa in oscars and blue gouramis, and at 160 dpa in white convicts. Subsequently, fish were killed in 300 mg/L MS-222 (Sigma), fixed in 4% PFA in PBS, and stored in 100% ethanol. Pectoral fin regeneration was documented with a Canon PowerShot SX510 HS camera for oscars and with a SMZ1000 stereoscope (Nikon) for the other fishes.

Library Preparation and Illumina Sequencing. For transcriptome sequencing, total RNA from different tissues was extracted using TRIzol Reagent (Life Technologies). A 2-step protocol, with the RNeasy Mini Kit (Qiagen) and DNasel treatment (Qiagen), was used to purify the RNAs and remove residual DNA. mRNA sequencing libraries were constructed using TruSeq RNA Library Prep Kit v2 or the TruSeq Stranded mRNA Library Prep (Illumina). Polypterus and axolotl reference transcriptomes and transcript abundance estimation were obtained from the sequencing of 3 biological replicates of blastemas at 3 dpa (Polypterus, 3 pools of 4 fin pairs), at 9 dpa (Polypterus, 3 pools of 2 fin pairs), at 14 dpa (axolotl, 3 pools of 2 limb pairs), and 3 biological replicates of UFs or ULs, performed on an Illumina 2500 Hiseq platform or Illumina NextSeq 500 with 100-bp paired-end reads (NCBI Sequence Read Archive project nos. PRJNA480693 and PRJNA480698).

Bioinformatic Analysis. Polypterus and axolotl reference transcriptomes were assembled de novo using Trinity with default parameters (50) (SI Appendix, Fig. S3 A-D). For each run, all read datasets were mapped to reference transcriptomes using CLC genomic workbench with default parameters (Qiagen). For comparison between runs, expression data per transcript were summed by human homolog gene cluster (HHGC) using a bash script. As previously described (41), the HHGCs were defined by grouping transcripts with an e-value of 10^{-3} when compared by BLASTx against the Human NCBI RefSeq database (11/2016). For each HHGC, the expression was calculated in TPM, and the comparison was based on t test considering 2 conditions (EFB/FB/ LB and UF/UL) with 3 independent biological replicates. A similarity matrix between runs shown in SI Appendix, Fig. S3E was calculated using TPM values for each Human Cluster Gene, a log₂ and z-score transformation, and Spearman rank correlation in Morpheus software (https://software.broadinstitute.org/ morpheus). A list of enriched GO terms was produced using the Gene Ontology Consortium web-based tool (51, 52). DEGs with false-discovery rate (FDR)-adjusted P values smaller than 0.05 were ranked from highest to lowest fold-change (FC) values, and the corresponding ranked list of gene symbols was used for GO enrichment analysis. GO enriched categories were significant when P values were 0.05 or less. Reactome pathway overrepresentation was assessed using the Reactome web-based analysis tool, providing a gene list as input (53, 54), and then ranking results according to the overrepresentation score. Venn diagrams were generated using BioVenn (55).

Corroboration of Axolotl DGE Datasets by Comparison with Publicly Available Data. Five runs were downloaded from publicly available axolotl RNA-seq runs (21). Three were from RNA-seq of axolotl nonregenerating upper arm tissue (SRR2885871, SRR2885875, SRR2885873) and 2 of a proximal blastema (SRR2885866, SRR2885865). Each run was mapped on our axolotl reference transcriptome using CLC genomic workbench with default parameters (Qiagen), and expression data in TPM was calculated by HHGC

Interspecies Transcriptome Comparisons. The overlap between up-regulated genes in blastemas of 9-dpa Polypterus and 14-dpa axolotl was tested using z-scores. One-thousand random subsets of the same size sampled from the Polypterus reference transcriptome were generated (https://github.com/ marcosp-sousa/matapi). Because this set follows a normal distribution (Shapiro-Wilk normality P < 2.2e-16), z-scores were used for statistical significance. The 2-tailed P value from Fig. 3C was obtained using the normal distribution function in R [2*pnorm(abs(Polypterus 9 dpa Z-score), lower.tail = F)]. Enrichment of the regeneration profile of axolotl limb at 14 dpa in the Polypterus regeneration profile at 9 dpa (Fig. 3D) was calculated using GSEA desktop application (http://software.broadinstitute.org/gsea/index.jsp). ScRNA-seq data tables containing TPM values from a previous study on axolotl regeneration (28) were used for cross-species comparison of appendage regeneration profiles. FC values from each stage of axolotl limb regeneration or limb development was calculated by directly dividing mean expression values (TPM) of a given gene by the corresponding value in the UL. From these mock transcriptomes, lists of up-regulated genes with FC > 4 were used for GSEA comparisons and lists of up-regulated genes with FC > 2 were used for other comparisons. A heatmap of GSEA enrichment scores, shown in Fig. 4D, was generated with log₂ and z-score transformed values in Morpheus software (https://software.broadinstitute.org/morpheus).

qPCR. Polypterus blastemas of 9 dpa and UF were used for RNA extraction and subsequent DNase treatment and purification, performed as described for RNA-seq library preparation. Left and right pectoral fins at 9 dpa of 1 animal were used in each biological replicate. For UF, the proximal region of 1 pectoral fin with the rays removed was used in each biological replicate. cDNA was prepared using the SuperScript III First-Strand Synthesis SuperMix (Thermo Fisher Scientific) with 0.5 μg of total RNA and oligo dT primers. Gene-specific oligos for qPCR assays were designed using Primer Express Software v3.0 (Thermo Fisher Scientific) and used in a final concentration of 200 nM to each primer. qPCR was carried out using GoTaq Probe qPCR Master Mix (Promega) in a final volume of 10 μ L, in a StepOnePlus Real-Time PCR System (Applied Biosystems), as previously described (6). Relative mRNA expressions were calculated using the $2^{-\Delta\Delta CT}$ method (56). ΔCTs were obtained from CTs normalized with Tubb levels in each sample. Each qPCR determination was performed with 2 (UF) to 3 (9 dpa) biological and 3 technical replicates. Expression in Polypterus UF (mean value of 2 biological replicates) was used as a reference to obtain relative expression levels in the regeneration time point of 9 dpa. Oligos used are provided in SI Appendix, Table S1.

Histology and in Situ Hybridization. Regenerating fins of Polypterus at 3 dpa (n = 2) and 9 dpa (n = 2) were sampled, embedded, and frozen in OCT (TissueTek). Frozen sections (20 μ m) were obtained on a Leica CM1850 UV cryostat and positioned on Color Frost Plus microscope slides (Thermo Fisher Scientific). Sections were fixed as previously described (6), and stored at -80 °C for H&E staining or in situ hybridization. Riboprobe templates for in situ hybridization were produced by a 2-round PCR strategy: first-round PCR produced specific fragments (400-500 bp) of selected genes and in a second PCR a T7 promoter sequence was included at either 5'or 3'end of the fragments for generation of templates for sense or antisense probes. Primers are listed in SI Appendix, Table S2. The riboprobes were synthesized using T7 RNA polymerase (mMESSAGE mMACHINE Transcription kits, Ambion) and DIG-labeling mix (Roche). In situ hybridization was performed as previously described (57), using 300 ng of DIG-labeled riboprobe per slide. Slides were photographed on Nikon Eclipse 80i microscope and the images were processed on the NIS-Element D4.10.1 program.

Statistical Analysis. For each transcript and HHGC, mean TPM value between UF/UL and EFB/FB/LB conditions was compared with a 2-tailed t test. A transcript or HHGC is classified as differentially expressed when its FC is superior to 2 or inferior to -2 and FDR-adjusted P value is inferior to 0.05. GO enrichment and Reactome pathway overrepresentation analyses were performed using the GO Consortium and Reactome web-based tools, using Fishers exact P value or a statistical (hypergeometric distribution) test, respectively, gPCR analysis data were analyzed using a 2-tailed Welch's corrected t test using GraphPad Prism v5.0 for Windows (GraphPad Software). GSEA P values were estimated with 1,000 permutations.

Data and Materials Availability. All data are available in the main text or SI Appendix.

ACKNOWLEDGMENTS. We thank Daniele Salgado, Louise Perez, and Mariana Dias for technical asistance; Chris Amemiya and George Mattox for insightful comments on the manuscript; Osage Catfisheries Inc. and the Kahrs family for their continued support of paddlefish research; Allyse Ferrara and Ouenton Fontenot (Nicholls State University) for gar spawns: Carrie Kozel, Brett Racicot, and Solomon David for gar husbandry at Michigan State University; and John H. Postlethwait, Trevor Enright, and the University of Oregon Aquatics Facility team for support with initial gar fin regeneration trial experiments at the University of Oregon. This work was supported by funding from Conselho Nacional de Pesquisas Universal Program Grant 403248/2016-7 and Comissao de Aperfeiçoamento de Pessoal de Nival Superior/Alexander von Humboldt Foundation fellowship (to I.S.), and a postdoctoral fellowship from Conselho Nacional de Pesquisas (to A.D.).

- M.C.D. thanks research support from the National Science Foundation (IOS 1853949). I.B. thanks support from NIH R010D011116 for gar experiments. G.O. receives funding from Conselho Nacional de Pesquisas (307479/2016-1), Comissao de Aperfeiçoamento de Pessoal de Nival Superior (88887.130628/2016-00), and GCRF-RCUK (BB/P027849/1-CABANA). This study was financed in part by the Coordenação de Aperfeiçoamento de Pessoal de Nível Superior, Brasil Finance Code 001.
- M. I. Coates, R. Marcello, M. Friedman, Ever since Owen: Changing perspectives on the early evolution of tetrapods. Annu. Rev. Ecol. Evol. Syst. 39, 571–592 (2008).
- M. C. Davis, The deep homology of the autopod: Insights from hox gene regulation. Integr. Comp. Biol. 53, 224–232 (2013).
- 3. I. Schneider, N. H. Shubin, The origin of the tetrapod limb: From expeditions to enhancers. *Trends Genet.* **29**, 419–426 (2013).
- 4. A. Simon, E. M. Tanaka, Limb regeneration. Wiley Interdiscip. Rev. Dev. Biol. 2, 291–300 (2013).
- J. P. Brockes, P. B. Gates, Mechanisms underlying vertebrate limb regeneration: Lessons from the salamander. Biochem. Soc. Trans. 42, 625–630 (2014).
- A. F. Nogueira et al., Tetrapod limb and sarcopterygian fin regeneration share a core genetic programme. Nat. Commun. 7, 13364 (2016).
- J. N. Dent, Limb regeneration in larvae and metamorphosing individuals of the South African clawed toad. J. Morphol. 110, 61–77 (1962).
- N. B. Fröbisch, C. Bickelmann, J. C. Olori, F. Witzmann, Deep-time evolution of regeneration and preaxial polarity in tetrapod limb development. *Nature* 527, 231–234 (2015).
- N. B. Frobisch, C. Bickelmann, F. Witzmann, Early evolution of limb regeneration in tetrapods: Evidence from a 300-million-year-old amphibian. *Proc. Biol. Sci.* 281, 20141550 (2014).
- D. B. Amaral, I. Schneider, Fins into limbs: Recent insights from sarcopterygian fish. Genesis 56, e23052 (2018).
- M.-A. Akimenko, M. Marí-Beffa, J. Becerra, J. Géraudie, Old questions, new tools, and some answers to the mystery of fin regeneration. Dev. Dyn. 226, 190–201 (2003).
- F. Galis, G. P. Wagner, E. L. Jockusch, Why is limb regeneration possible in amphibians but not in reptiles, birds, and mammals? Evol. Dev. 5, 208–220 (2003).
- J. Shao, X. Qian, C. Zhang, Z. Xu, Fin regeneration from tail segment with musculature, endoskeleton, and scales. J. Exp. Zoolog. B Mol. Dev. Evol. 312, 762–769 (2009).
- R. Cuervo, R. Hernández-Martínez, J. Chimal-Monroy, H. Merchant-Larios, L. Covarrubias, Full regeneration of the tribasal Polypterus fin. *Proc. Natl. Acad. Sci. U.S.A.* 109, 3838–3843 (2012).
- A. I. Nikiforova, V. A. Golichenkov, [Characteristics of the reparative regeneration of fins in the polypterid fish (Polypteridae, Actinopterygii)] [in Russian]. Ontogenez 43, 136–142 (2012)
- R. Betancur-R et al., Phylogenetic classification of bony fishes. BMC Evol. Biol. 17, 162 (2017).
- L. C. Hughes et al., Comprehensive phylogeny of ray-finned fishes (Actinopterygii) based on transcriptomic and genomic data. Proc. Natl. Acad. Sci. U.S.A. 115, 6249– 6254 (2018).
- S. Darnet et al., Deep evolutionary origin of limb and fin regeneration. NCBI Sequence Read Archive. https://www.ncbi.nlm.nih.gov/bioproject/PRJNA480698. Deposited 11 July 2018.
- S. Darnet et al., Deep evolutionary origin of limb and fin regeneration. NCBI Sequence Read Archive. https://www.ncbi.nlm.nih.gov/bioproject/PRJNA480693. Deposited 11 July 2018.
- C. McCusker, S. V. Bryant, D. M. Gardiner, The axolotl limb blastema: Cellular and molecular mechanisms driving blastema formation and limb regeneration in tetrapods. Regeneration (Oxf.) 2, 54–71 (2015).
- D. M. Bryant et al., A tissue-mapped axolotl de novo transcriptome enables identification of limb regeneration factors. Cell Rep. 18, 762–776 (2017).
- J. R. Monaghan et al., Microarray and cDNA sequence analysis of transcription during nerve-dependent limb regeneration. BMC Biol. 7, 1 (2009).
- C. H. Wu, M. H. Tsai, C. C. Ho, C. Y. Chen, H. S. Lee, De novo transcriptome sequencing of axolotl blastema for identification of differentially expressed genes during limb regeneration. *BMC Genomics* 14, 434 (2013).
- D. Knapp et al., Comparative transcriptional profiling of the axolotl limb identifies a tripartite regeneration-specific gene program. PLoS One 8, e61352 (2013).
- S. R. Voss et al., Gene expression during the first 28 days of axolotl limb regeneration I: Experimental design and global analysis of gene expression. Regeneration (Oxf.) 2, 120–136 (2015).
- B. J. Haas, J. L. Whited, Advances in decoding axolotl limb regeneration. Trends Genet. 33, 553–565 (2017).
- 27. E. Nacu, E. M. Tanaka, Limb regeneration: A new development? *Annu. Rev. Cell Dev. Biol.* 27, 409–440 (2011).
- 28. T. Gerber et al., Single-cell analysis uncovers convergence of cell identities during axolotl limb regeneration. Science 362, eaaq0681 (2018).
- S. L. Tsai, C. Baselga-Garriga, D. A. Melton, Blastemal progenitors modulate immune signaling during early limb regeneration. *Development* 146, dev169128 (2019).
- J. W. Godwin, A. R. Pinto, N. A. Rosenthal, Macrophages are required for adult salamander limb regeneration. *Proc. Natl. Acad. Sci. U.S.A.* 110, 9415–9420 (2013).

- N. W. Al Haj Baddar, A. Chithrala, S. R. Voss, Amputation-induced reactive oxygen species signaling is required for axolotl tail regeneration. *Dev. Dyn.* 248, 189–196 (2019).
- 32. N. R. Love et al., Amputation-induced reactive oxygen species are required for successful Xenopus tadpole tail regeneration. Nat. Cell Biol. 15, 222–228 (2013).
- M. Zhang et al., Melanocortin receptor 4 signaling regulates vertebrate limb regeneration. Dev. Cell 46, 397–409.e5 (2018).
- S. J. Odelberg, A. Kollhoff, M. T. Keating, Dedifferentiation of mammalian myotubes induced by msx1. Cell 103, 1099–1109 (2000).
- C. M. Arenas Gómez, R. M. Woodcock, J. J. Smith, R. S. Voss, J. P. Delgado, Using transcriptomics to enable a plethodontid salamander (Bolitoglossa ramosi) for limb regeneration research. *BMC Genomics* 19, 704 (2018).
- M. Suzuki, A. Satoh, H. Ide, K. Tamura, Nerve-dependent and -independent events in blastema formation during Xenopus froglet limb regeneration. *Dev. Biol.* 286, 361– 375 (2005).
- R. N. Christensen, M. Weinstein, R. A. Tassava, Expression of fibroblast growth factors 4, 8, and 10 in limbs, flanks, and blastemas of Ambystoma. *Dev. Dyn.* 223, 193–203 (2002).
- D. Nishimura et al., Roles of ADAM8 in elimination of injured muscle fibers prior to skeletal muscle regeneration. Mech. Dev. 135, 58–67 (2015).
- M. Dentice et al., Intracellular inactivation of thyroid hormone is a survival mechanism for muscle stem cell proliferation and lineage progression. Cell Metab. 20, 1038–1048 (2014).
- K. B. Umansky et al., Runx1 transcription factor is required for myoblasts proliferation during muscle regeneration. PLoS Genet. 11, e1005457 (2015).
- R. Stewart et al., Comparative RNA-seq analysis in the unsequenced axolotl: The oncogene burst highlights early gene expression in the blastema. PLoS Comput. Biol. 9, e1002936 (2013).
- G. B. Stock, S. V. Bryant, Studies of digit regeneration and their implications for theories of development and evolution of vertebrate limbs. *J. Exp. Zool.* 216, 423–433 (1981).
- G. P. Wagner, B. Y. Misof, Evolutionary modification of regenerative capability in vertebrates: A comparative study on teleost pectoral fin regeneration. *J. Exp. Zool.* 261, 62–78 (1992).
- 44. S. Lu et al., Bichirs employ similar genetic pathways for limb regeneration as are used in lungfish and salamanders. Gene 690, 68–74 (2019).
- C. Chiang et al., Cyclopia and defective axial patterning in mice lacking Sonic hedgehog gene function. Nature 383, 407–413 (1996).
- G. F. Stopper, G. P. Wagner, Inhibition of Sonic hedgehog signaling leads to posterior digit loss in Ambystoma mexicanum: Parallels to natural digit reduction in urodeles. Dev. Dyn. 236, 321–331 (2007).
- B. N. Singh, M. J. Doyle, C. V. Weaver, N. Koyano-Nakagawa, D. J. Garry, Hedgehog and Wnt coordinate signaling in myogenic progenitors and regulate limb regeneration. *Dev. Biol.* 371, 23–34 (2012).
- E. Nacu, E. Gromberg, C. R. Oliveira, D. Drechsel, E. M. Tanaka, FGF8 and SHH substitute for anterior-posterior tissue interactions to induce limb regeneration. *Nature* 533, 407–410 (2016).
- M. C. Davis, N. H. Shubin, A. Force, Pectoral fin and girdle development in the basal actinopterygians Polyodon spathula and Acipenser transmontanus. J. Morphol. 262, 608–628 (2004).
- B. J. Haas et al., De novo transcript sequence reconstruction from RNA-seq using the Trinity platform for reference generation and analysis. Nat. Protoc. 8, 1494–1512 (2013)
- M. Ashburner et al.; The Gene Ontology Consortium, Gene ontology: Tool for the unification of biology. Nat. Genet. 25, 25–29 (2000).
- H. Mi et al., PANTHER version 11: Expanded annotation data from gene ontology and reactome pathways, and data analysis tool enhancements. Nucleic Acids Res. 45, D183–D189 (2017).
- A. Fabregat et al., The reactome pathway knowledgebase. Nucleic Acids Res. 46, D649–D655 (2018).
- 54. K. Sidiropoulos et al., Reactome enhanced pathway visualization. *Bioinformatics* 33, 3461–3467 (2017).
- T. Hulsen, J. de Vlieg, W. Alkema, BioVenn—A web application for the comparison and visualization of biological lists using area-proportional Venn diagrams. BMC Genomics 9, 488 (2008).
- K. J. Livak, T. D. Schmittgen, Analysis of relative gene expression data using real-time quantitative PCR and the 2(-Delta Delta C(T)) method. Methods 25, 402–408 (2001).
- J. L. de Lima et al., A putative RA-like region in the brain of the scale-backed antbird, Willisornis poecilinotus (Furnariides, Suboscines, Passeriformes, Thamnophilidae). Genet. Mol. Biol. 38, 249–254 (2015).